Energy & Buildings 251 (2021) 111388

Contents lists available at ScienceDirect

Energy & Buildings

journal homepage: www.elsevier.com/locate/enb

Probing the historic thermal and humid environment in a 2000-year-old ancient underground tomb and enlightenment for cultural heritage protection and preventive conservation

Jing Xiong [a,b], Angui Li [b,*], Changping Liu [b], Jungang Dong [c], Bin Yang [b,d], Junji Cao [e], Tong Ren [b]

[a] School of Environmental and Municipal Engineering, Xi'an University of Architecture and Technology, Xi'an, Shaanxi Province, China
[b] School of Building Service Science and Engineering, Xian University of Architecture and Technology, Xi'an, Shaanxi Province, China
[c] School of Architecture, Xian University of Architecture and Technology, Xi'an, Shaanxi Province, China
[d] Department of Applied Physics and Electronics, Umeå University, Umeå, Sweden
[e] Key Lab of Aerosol Chemistry & Physics, Institute of Earth Environment, Chinese Academy of Sciences, Xi'an, Shaanxi Province, China

ARTICLE INFO

Article history:
Received 14 March 2021
Revised 17 August 2021
Accepted 20 August 2021
Available online 24 August 2021

Keywords:
Underground ancient tomb
Temperature
Relative humidity
Variation
Field test
CFD

ABSTRACT

The development and utilization of urban underground space have contributed to more excavation of ancient tombs in recent years. The microclimate in the burial environment is crucial for the sustainability of historical artifacts. In this paper, the variation in thermal and humid conditions during the burial time from the closure of a tomb to excavation was investigated by field testing and computational fluid dynamics (CFD) modeling. The selected object is the famous M1 tomb chamber of the mausoleum Zhang An-shi, which has a 2000-year history. It was found that the average air temperature (T) and relative humidity (RH) of the M1 tomb chamber before excavation were 12.7 °C and 93.0%, respectively. The results of the CFD simulation suggest that the burial time of an ancient tomb consists of a very short variable phase and a long stable phase. The very beginning phase may be as short as 0.3 h. The dramatic changes in temperature and RH were more than 10 °C and 20%, respectively. Consequently, dramatic changes in the thermal and humid environment will trigger the deterioration of historical artifacts. Current findings further suggest that the local annual average temperature is optimal for the conservation of underground artifacts excavated from the soil thermostatic layer. This study paves the way for characterizing the environment of an ancient tomb chamber, as well as museum design, energy savings that support cultural heritage protection and preventive conservation.

1. Introduction

To promote the coordinated and healthy development of the urban economic and social environment, the development and use of underground space is of great significance to urban development. Underground space offers an effective means to alleviate the prominent contradictions and problems in urban development [1,2]. During the rapid development of underground space, an increasing number of underground ancient tombs were discovered, particularly in China, which has five thousand years of history. The archaeological excavation area of China in 2018 reached 1400×10^4 m^2 [3], as shown in Fig. 1. Underground historical artifacts and their burial places (e.g., caves, necropolises, monuments, catacombs, tombs, crypts) are the precious heritage of human civilizations [4–6].

There are generally two ways to preserve excavated cultural relics: indoor-display museums or archaeological museums [7,8]. Indoor-display museums are traditional museums where movable cultural relics from another location are collected and preserved. Archaeological museums mainly focus on the immovable historical sites [9]. Temperature and RH are the key control parameters in both storage situations [10,11]. Inappropriate temperature and RH can cause mechanical, biological and chemical degradation of cultural relics [12,13]. For organic materials, temperature can accelerate chemical degradation [10]. Absorption or evaporation of water makes cultural relics swell or warp, particularly relics made from different materials because of their different expansion coefficients, such as panel paintings and lacquered wood. High RH will cause the corrosion of metals and the fading of dyes and the weakening of paper and textiles [14]. Paintings on canvas can be irreversibly damaged by moisture: humidity fluctuations of the

* Corresponding author at: No.13, YantaStreet, Beilin District, Xi'an 710055, China.
E-mail address: Liag@xauat.edu.cn (A. Li).

https://doi.org/10.1016/j.enbuild.2021.111388
0378-7788/

Nomenclature

T	temperature, °C	T_f	temperature of fluid, °C
RH	relative humidity, %	ΔT	difference between t_w and t_f
Δt	time step, s	T_m	average temperature of boundary layer, °C
Δx	length of mesh, m	l	height of wall, m
u	air velocity, m/s	v	kinematic viscosity, m^2/s
CFL	Courant number	ω	initial mass fraction of water vapor
Ra	Rayleigh number	m_v	mass of water vapor, g
Gr	Grashof number	m_a	mass of dry air, kg
Pr	Prandtl number	d	moisture content, g/kg
g	gravitational acceleration, m/s^2		
a	coefficient of cubical expansion, 1/K		
T_w	temperature of wall, °C		

ambient environment, condensation of liquid water on the surface, liquid water or water vapor existing in conservation treatments [15]. Thermo-hygrometric cycles have a considerable influence on organic materials, particularly rapid fluctuation. Dimensional variations occur due to steep gradients starting from the outer surface of the object, resulting in irreversible damage [16]. Changes in relative humidity pose the greatest threat to wooden historical artifacts [17]. Moisture accumulation will promote the growth of microorganisms on cultural relics [18]. Humidity is also positively correlated with fungal richness [19]. *Penicillium* and *Aspergillus* genera caused black spots in two 1700-year-old tombs [20]. *Bacillus* strains produce white deposition, causing frescoes' deterioration [21]. Violet stains on the walls of a Roman tomb were produced by *Streptomyces parvus* [22]. The Crypt of the Cattedrale di Otranto suffered from several forms of decay, such as mildew, efflorescence and molds because porous materials easily maintain water and/or moisture [23].

To reduce the damage caused by temperature and RH on precious cultural relics, a series of standards have been issued. AICCM 2014, the UK standard 2012, ASHRAE 2011 and GB/T 18883–2002 specify the appropriate temperature and RH and their fluctuation range for preservation of cultural relics in museums [24–26]. Heating, ventilation and air conditioning (HVAC) systems are the primary method to fulfill thermal and humid requirements [27,28]. Tempering heating systems, which refer to wall heating through pipes, were adopted to create a stable environment in museum buildings [29]. An air curtain system was proposed to control the local environment of an archaeological museum by isolating relics from the exhibition hall [30–32]. The air inlet/outlet positions were optimized to improve the performance of the abovementioned advanced air curtain system [8]. The period with small fluctuations of RH in the warm season increased from 2% to 88% through improved control schemes of the HVAC system in a typical museum [33].

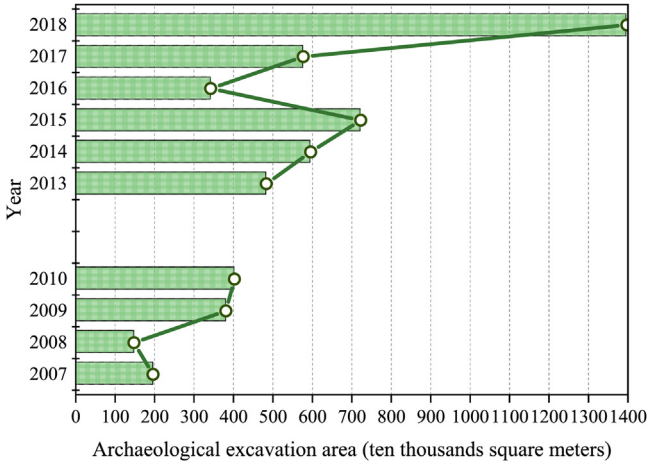

Fig. 1. Archaeological excavation area records of China over the years.

However, even if excavated cultural relics can be stored in a museum where the HVAC system is in perfect operating condition and satisfies the microclimate requirements, secondary damage is still unavoidable. Unearthed cultural relics have adapted to their burial environment after thousands of years of burial. Numerous historical artifacts are in excellent condition even after centuries of burial [34,35]. It is widely believed that the outstanding preservation of unearthed historical artifacts is due to the exceptional stability of the interior climate parameters in the subsurface environment [36,37]. Thermal and humid conditions in the burial environment were considered essential factors to the integrity of historical artifacts. If cultural relics are excavated suddenly, the severe fluctuation of temperature and RH will cause irreversible deformations, such as curling and cracks. At the beginning of excavation, Terra Cotta Warriors were intact and decorated with colorful drawings. Unfortunately, the underlying raw lacquer suffered from serious cock, crimp, scaling and flaking, exposing the gray layer only a few hours after excavation [38]. Thus, it is meaningful to study the thermal and humid environment of cultural relics before excavation. It can be an important basis of preventive conservation to avoid and minimize decay [39].

Although research on burial environments has made progress [40–44], the number of such studies remains limited, particularly studies on the variation in the thermo-hygrometric environment during burial time and its influence on historical artifacts in an intact subsurface environment. Based on measured environmental data before excavation, the present paper simulated and analyzed the microenvironmental changes that occurred in ancient underground tombs for up to two thousand years and provided an important scientific basis for the preventive protection of cultural relics.

2. Methods

Both CFD modeling and field-testing methods have been applied to investigate thermal and humid environments in a 2000-year-old underground tomb chamber. Compared to field testing, CFD simulation is capable of providing 3D high-resolution thermo-hygrometric data indoors [45]. Advanced CFD techniques are able to address the specificity of such topics, provide useful decision-making support to optimize the preservation environment of historical relics, and provide a suitable environment for visitors. In the Senate Room at Palazzo Madama in Turin (Italy), CFD was applied to provide an optimal ventilation strategy

[46]. A three-dimensional CFD model was developed to assess the adequacy of natural ventilation in a historical building, located in southern Italy [47]. A prototype meshing tool is developed to construct adaptive quadrilateral meshes from two-dimensional image data, e.g., architectural drawings [48]. CFD was applied to simulate the ventilation of the pharaonic tombs of the Valley of Kings, Luxor, Egypt [49]. For cultural heritage protection in the Palatina Library, numerical simulation was applied to determine the moisture, temperature and air velocity fields in the indoor microclimatic study [50]. In the Lascaux cave, the Eulerian/Lagrangian method was used to numerically simulate incompressible convection flows with complex obstacles [51].

2.1. Physical model and site description

The M1 tomb chamber of the mausoleum of Zhang An-shi is a typical ancient Chinese tomb dating to the Han Dynasty, which has a long history of 2000 years. It is situated in southern Xi'an, which used to be the capital of the Han Dynasty (Fig. 2a). As the capital of thirteen ancient dynasties, many large royal or noble tombs were buried in Xi'an. The mausoleum of Zhang An-shi is a high-grade Han noble tomb with an area of approximately 40000 m^2. As the most distinctive chamber, the M1 tomb chamber was never plundered or damaged. Hence, the burial chamber was nearly intact when it was discovered in 2011. Several painted lacquers, lacquers with copper and lacquers with gold and silver hoops were excavated from the M1 tomb chamber [52]. It is rare for a tomb chamber such as M1 to be intact because most underground ancient tombs have been disturbed and the original tomb environment is defunct [53]. The M1 tomb chamber consists of an opening, a west-to-east passage and a chamber. The opening is located at the west end of the passage, and the chamber is located at the east end of the passage. The chamber is surrounded by layers of bricks. The tomb chamber floor is 9.0 m below ground level (Fig. 2b), with a length of 4.0 m, width of 1.5 m and height of 2.0 m (Fig. 2c, d) [52].

2.2. Field-testing procedure

Before the M1 tomb chamber was excavated, microclimatic parameters (T and RH) and atmospheric components (O_2, CO_2, methane [CH_4], and carbon monoxide [CO]) were measured inside the chamber with online monitoring systems from 10:01 a.m. to 14:20 p.m. on April 7, 2011, as shown in Fig. 3. To our knowledge, this study marks the first time that microclimatic parameters and atmospheric components inside an ancient tomb chamber have been monitored in China before the tomb chamber is excavated. The original burial environment is highly valuable. Every item was monitored for 15 to 30 min with a logging interval of 5 min. First, a sampling hole of approximately 1 cm in diameter was dug at the appropriate gap on the brick door. After inserting a polytetrafluoroethylene (PTFE) tube (0.63 cm in outer diameter and 3 m in length) into the sampling hole, the gap between the tube and the sampling hole was sealed rapidly with PTFE tape. Second, an aspirator pump of LFG 20 (ADC Gas Analysis Limited, Herts, UK) aspirated the gas in the tomb through the PTFE tube and measured the gas in real time. The sampling flow rate was 0.2 L·min^{-1}. The technical characteristics of LFG 20 are presented in Table 1. After the abovementioned monitoring, the diameter of the sampling hole was expanded to 5 cm. The Q-Trak sensor (Model 7565, TSI Incorporated, Shoreview, MN, USA) was then inserted into the hole to monitor T, RH, CO and CO_2. The gap between the expansion link of the Q-Trak and the sampling hole was sealed rapidly with PTFE tape [53]. The technical characteristics of the Q-Trak are shown in Table 2.

2.3. CFD model and numerical simulation

For this simulation, a 3D CFD model based on the Navier–Stokes (RANS) equations was used to simulate the formation of temperature and relative humidity through ANSYS©FLUENT (version R 16.1). The model was built using the original dimensions of the M1 tomb chamber, which is shown in Fig. 2e, and the grid mesh

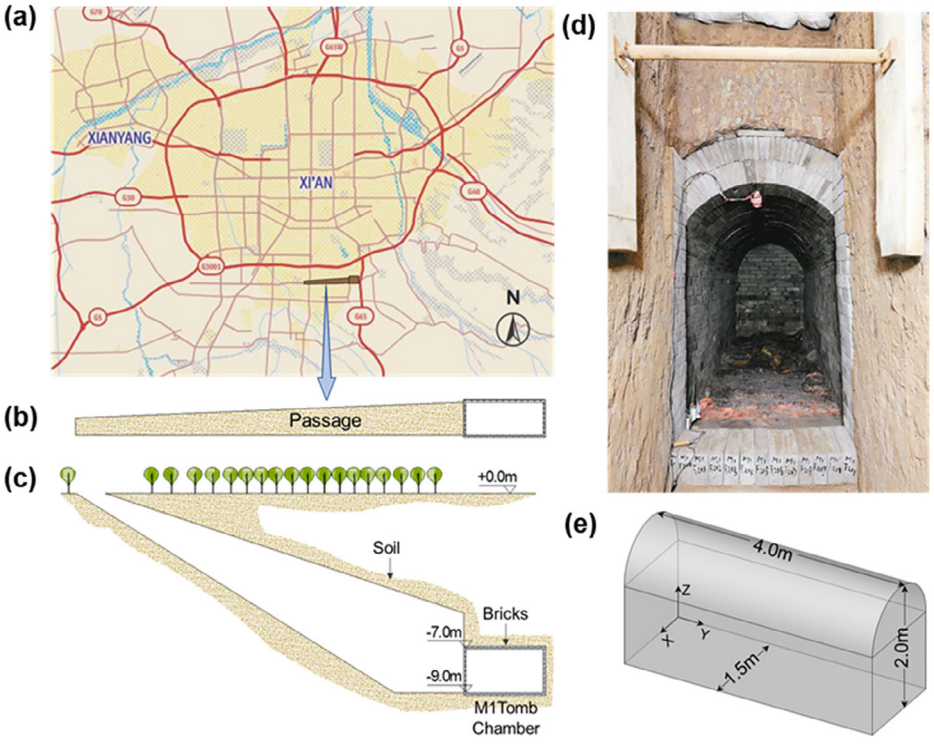

Fig. 2. M1 tomb chamber of the mausoleum Zhang An-shi. (a) The tomb is located in southwestern Xi'an, China, (b) Planform of the M1 tomb chamber, (c) Vertical sketch of the M1 tomb chamber including stratigraphic location and envelope enclosure, (d) A photo of the M1 tomb chamber, (e) Schematic diagram of the M1 tomb chamber.

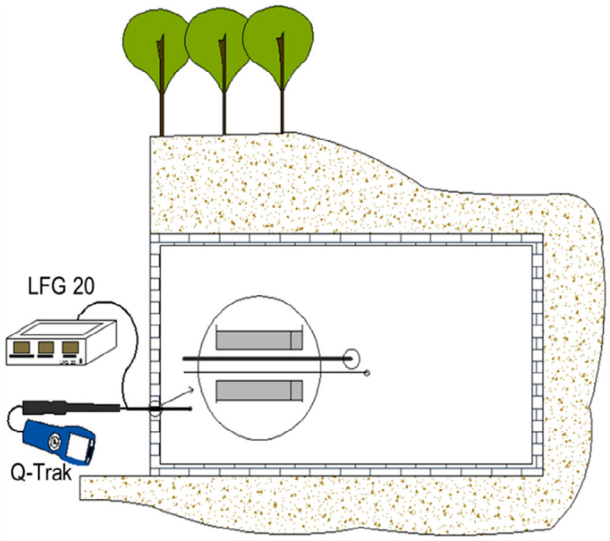

Fig. 3. Schematic diagram of the monitoring process and rigs.

Table 1
Technical characteristics of the LFG 20 [54].

	CO_2	CH_4	O_2
Measurement technique	Non-dispersive infrared absorption	Non-dispersive infrared absorption	Electrochemical cell
Range	0–10.00%	0–100.0%	0–25%
Precision	±0.5%	0–10.0%, ±0.5% 10–100%, ±3.0%	±0.4%

of a typical plane is presented in Fig. 4. The semi-implicit method for the pressure-linked equations (SIMPLE) algorithm was selected for pressure and velocity field coupling, and the second order upwind discretization scheme was chosen to solve the variables in the simulation cases. The energy equation was solved. Humidity was tracked by species transport model. The mass fraction of water vapor was calculated from the enthalpy-humidity chart and was set as the initial condition. The other gaseous components were not simulated by CFD. The time step is set as 4 s in this manuscript according to the following equation:

$$\Delta t = \frac{(\mathrm{CFL})\Delta x}{u} \approx 4\ s \tag{1}$$

where Δt is the time step, s, CFL is the Courant number, Δx is the length of the mesh, and u is the air velocity, m/s.

The numerical simulation was based on the assumption that air flow in the tomb chamber could be considered incompressible and laminar due to the low velocity. Airflow in the underground tomb was natural convection. The Rayleigh criterion is the criteria basis for the flow regime, which is defined as Equation (2). When $Ra = Gr \cdot \mathrm{Pr} \geqslant 10^9$, the flow is turbulent [56].

$$Ra = Gr \cdot \mathrm{Pr} = \frac{g\alpha\Delta T l^3}{v^2} \cdot \mathrm{Pr} \tag{2}$$

where Ra is the Rayleigh number, Gr is the Grashof number, Pr is the Prandtl number, which is generally 0.7 for air, g is the gravitational acceleration, 9.81 m/s^2, a is coefficient of cubical expansion, 1/K, ΔT is the difference between T_w and T_f, °C, T_w is the temperature of the wall, °C, T_f is the temperature of the fluid, °C, l is the height of the wall, and ν is the kinematic viscosity, m^2/s.

$T_m = \frac{T_w + T_f}{2}$, which is the average temperature of the boundary layer. The following is assumed:

When $T_f = -0.1$, $t_m = 6.8$, $\alpha = 0.00357$

When $l = 0.4H$, $Ra = 9.51 \times 10^8 \approx 10^9$

That is, if T_f is −0.1 °C, at a height of 0.8 m, the flow will become turbulent. However, because ΔT gradually decreases, the flow will remain laminar even at higher points. Therefore, in our simulation, the flow was set as laminar.

2.3.1. Initial and boundary conditions

Soil is a highly complicated environment. In the corrosion process, its chemical composition, geological parameters and hydrological factors play a significant role [57]. They are also important factors influencing the thermal and humid environment in tombs. The temperature of the soil thermostatic layer is stable throughout the year and is nearly identical to the average annual temperature of the ambient atmosphere [58,59]. In this paper, the M1 tomb chamber is located in the soil thermostatic layer as it is 9.0 m below ground level [59]. It had not been invaded by underground water or external environmental conditions. Therefore, when the M1 tomb chamber was closed at ~ 50 B.C. [60], the temperature of the tomb wall was the same as the annual atmospheric mean temperature of that year. Fig. 5 illustrates the temperature variation of China from 3000 B.C. to 1950 A.D. The annual mean air temperature in 1950 was used as a reference value and set as 0 °C. If the temperature in other years is higher than the temperature in 1950, the temperature variation is positive; conversely, if the temperature in a certain year is lower than the temperature in 1950, it is negative [61]. The annual mean air temperature at 50 B.C., when the tomb was buried, was approximately 1 °C higher than that in 1950 A.D. The annual mean air temperature in 1950 in Xi'an was 13.3 °C [62]. Consequently, the wall temperature should be approximately 14.3 °C. However, temperatures over 5000 years in China cover a large time span. There must be some errors. According to the China Integrated Meteorological Information Service System, the normal mean year air temperature from 1971 A.D. to 2000 A.D. was 13.7 °C, which was between 13.3 °C and 14.3 °C, and the accuracy was acceptable [63]. Therefore, basic climatic conditions of Xi'an from 1971 A.D. to 2000 A.D. were adopted in the present study (Table 3). As calculated from Table 3, the annual mean atmospheric temperature in Xi'an is 13.7 °C. Therefore, the temperature of all the walls was set as 13.7 °C.

Due to the long history of the M1 tomb chamber, it is difficult to judge the closure time. To conveniently investigate the influences of meteorological conditions on the evolution of temperature and relative humidity in the tomb, extreme meteorological conditions were adopted. The burial time is assumed to be the coldest month or the hottest month. Hence, the initial temperature and relative humidity after burying are the same as the values in the coldest

Table 2
Technical characteristics of the Q-Trak [55].

	T	RH	CO_2	CO
Sensor	Thermistor	Thin-film capacitor	Non-dispersive infrared (NDIR)	Electro-chemical
Range	0–60 °C	5–95%	0–5000 ppm	0–500 ppm
Precision	±0.6 °C	±3%	±3% of reading or ± 50 ppm, whichever is greater	±3% of reading or ± 3 ppm, whichever is greater

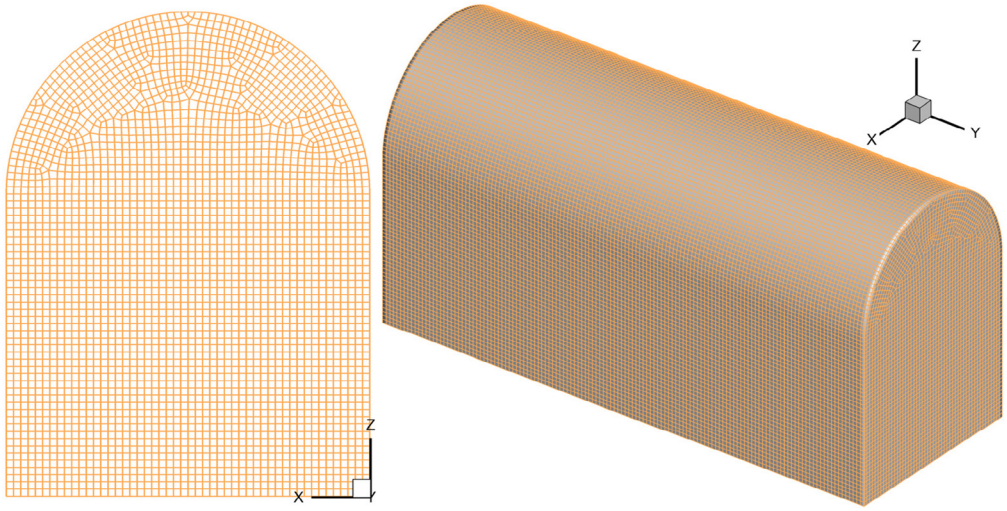

Fig. 4. The two- and three-dimensional grid mesh of a typical plane (Y = 2 m).

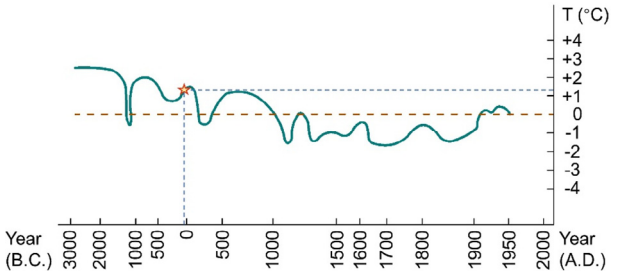

Fig. 5. Temperature variation in China from 3000 B.C. to 1950 A.D. [61] (The annual mean air temperature in 1950 is used as a reference value and set as 0 °C, shown by the orange dashed line. The green solid line indicates the average annual temperature fluctuation relative to 1950. The star refers to the annual average temperature in 50 B.C.) (For interpretation of the references to colour in this figure legend, the reader is referred to the web version of this article.)

month (January) or the hottest month (July). The initial air conditions are presented in Table 4. The initial moisture content is calculated using the enthalpy-humidity chart. The initial mass fraction of water vapor is calculated from the following equation:

$$\omega = \frac{m_v}{m_v + m_a} \tag{3}$$

where ω is the initial mass fraction of water vapor, m_v is the mass of water vapor, g, and m_a is the mass of dry air, kg.

$$d = \frac{m_v}{m_a} \tag{4}$$

where d is the moisture content, g/kg.

Thus,

$$\omega = \frac{dm_a}{dm_a + m_a} = \frac{d}{d+1} \tag{5}$$

2.3.2. Validation of the numerical model

Three types of grids were chosen to examine mesh independence to find a suitable grid with appropriate accuracy and using less simulation time. Therefore, according to the different ratios between the grid size and the overall model, three types of grids that have an order of magnitude gap are obtained. The relationship between grids of different orders of magnitude and simulation accuracy can be shown by the different orders of magnitude. It is helpful to quickly find a grid with high computational accuracy and short computation time. For this case, mesh configurations consist of 22650, 415492, and 1,414,800 cells. The mesh-independency examination results are presented in Fig. 6. The temperature and relative humidity of Point 1 (X = 0.75 m, Y = 2 m, Z = 0.4 m) in Pole BB_1 for these mesh configurations were compared. The maximum differences in temperature and relative humidity between the coarsest and finest meshes were approximately 3.1 °C and 3.9%, respectively. Nevertheless, a difference of 0.7 °C and 0.5% between the two finer meshes indicates that the second type of grid resulted in a mesh-independent solution.

To validate the presented numerical model, the measured data in Table 5 are compared with the simulation results. The average measured temperature is 12.7 °C, and the average measured relative humidity is 93%. According to Fig. 6, the temperature is stabilized at 13.7 °C, and the relative humidity is 90.2% in the CFD simulation. The ultimate stable air temperature in the CFD simulation is 7.8% higher than the measured air temperature in field testing. The final stable air relative humidity in the CFD simulation is 3.0% lower than the measured air relative humidity in field testing. These results indicate that the CFD method adopted in this study is reliable because the differences are less than 10%.

Table 4
Initial air conditions.

	Coldest month (Jan.)	Hottest month (Jul.)
Initial air temperature (°C)	−0.1	26.6
Initial relative humidity (%)	66	71
Initial moisture content (g/kg)	2.46	15.57
Initial mass fraction of water vapor	0.00245	0.01533

Table 3
Basic meteorological conditions of Xi'an (according to statistics from 1971 to 2000) [63].

	Jan.	Feb.	Mar.	Apr.	May	Jun.	Jul.	Aug.	Sep.	Oct.	Nov.	Dec.
Normal mean monthly air temperature (°C)	**−0.1**	2.9	8.1	14.8	19.8	24.8	**26.6**	25.3	19.9	13.9	6.9	1.3
Normal mean monthly relative humidity (%)	**66**	63	67	68	68	62	**71**	75	79	77	74	69

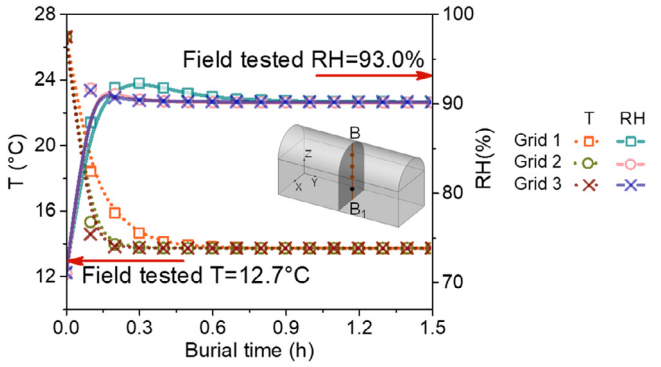

Fig. 6. Simulation results in three different grids in Point 1.

Table 5
Main microclimatic parameters of the M1 tomb chamber before excavation [53].

	T (°C)	RH (%)
Maximum	13.2	95.9
Minimum	12.4	86.7
Average value	12.7	93.0
Standard deviation	0.4	4.4

3. Results

3.1. Field testing and findings

Field monitoring of the main microclimatic parameters and atmospheric components for the M1 tomb chamber was conducted by a group of investigators [53]. The results of field monitoring of the M1 tomb chamber are presented in Table 5. The average indoor air temperature and relative humidity before excavation in 2011 were 12.7 °C and 93.0%, respectively. The standard deviations of temperature and relative humidity were 0.4 °C and 4.4%. The final stable atmospheric components inside the M1 tomb chamber are shown in Table 6. The average background value in Table 6 is based on references [64,65]. The average content of O_2 in the normal atmosphere is approximately 20.947% [64]. The global average background values of CO, CO_2 and CH_4 were obtained from multi-year monitoring records from 1992 to 2004 by the Waliguan Observatory [65]. The oxygen concentration (19.3 ± 0.1%) after a long burial was slightly lower than the global background value (20.9%). The concentration of CO_2 (432.7 ± 2.7 μmol·mol^{-1}) was thousands of times higher than the global background value (0.4 μmol·mol^{-1}). There was only a slight difference in CH_4 concentration between the measured value (1880.0 ± 25.2 nmol·mol^{-1}) and global background value (1814.4 nmol·mol^{-1}). Microbial deterioration is caused by aerobic or anaerobic decomposition processes. The final main gas product of aerobic decomposition processes is CO_2, while it is CH_4 for anaerobic decomposition processes. The findings of the field testing of atmospheric components inside the M1 tomb chamber suggest that aerobic decomposition processes mainly occurred during the burial time. The aerobic decomposition process occurred when oxygen was still abundant. This finding indicates that the changes in atmospheric components inside the ancient tomb resulted mainly from aerobic decomposition at the beginning stage of burial.

3.2. CFD simulation and analyses

3.2.1. Variations in temperature and relative humidity in the coldest month

Fig. 7 shows representative stratification phenomena of temperature and relative humidity of tomb air at 60 s, 360 s (0.1 h) and 1080 s (0.3 h) after sealing in the coldest month in two typical sections (X = 0.75 m and Y = 2 m). Clearly, temperature and relative humidity varied rapidly immediately after the tomb was sealed. The stratification phenomena disappear rapidly. The flow is asymmetric, although the geometry and boundary conditions are very symmetric. This result is comparable to the results of Wang et al. [66]. During the entire process, as shown in Fig. 7e, the velocity was very small. The direction of the vector was downward. Variations in the average temperature and relative humidity of the tomb air at four different heights (0.4 m, 0.8 m, 1.2 m, and 1.6 m) in the tomb chamber are shown in Fig. 8, which more obviously shows that the entire burial time consists of two phases: a variable phase and a stable phase. The variable phase was as short as 0.3 h. During the variable phase, the thermo-hygrometric conditions of tomb air were directly affected by soil temperature and soil moisture by heat and mass transfer. The soil moisture content is high, and it disperses constantly into the air by mass transfer. The relatively higher soil temperature increased the tomb air temperature by heating transfer. In this process, the stratification phenomenon appeared only in the vertical direction. The higher the height was, the higher the air temperature and relative humidity were. The reason for vertical stratification may be that there are only gravity and buoyancy forces in the vertical direction, but no other forces in the horizontal direction. The temperature of the tomb air close to the walls increases earlier, and then that air floats into the upper space. Cold air gradually subsided, which caused the temperature and relative humidity of the upper air to increase quickly, while causing those of the lower air to increase slowly. Because the density of water vapor is less than the density of tomb air, the moisture content of the upper air is higher than that of the lower air. The amplitude of the increase in moisture is higher than the amplitude of the increase in temperature in the upper higher space. Consequently, relative humidity increases with height in the variation phase. The closer to 0.3 h the phase was, the weaker the stratification phenomenon was. The energy in the chamber reached a balance before 0.3 h. Finally, the air temperature reached the same temperature as the wall, which was 13.7 °C. After 0.3 h, the temperature and relative humidity of tomb air were evenly distributed in the tomb. In the stable phase of burial time, burial remains lay in an almost constant thermo-hygrometric environment, if there was no other disturbance, such as plunder or underground water. The variation range of air temperature was 13.8 °C. The final relative humidity was 90.2%, and the variation range was 24.2%. There was no significant difference between the measured values and the final stable values of the simulation. This finding reflected the effective sealing of the M1 tomb chamber.

3.2.2. Variations in temperature and relative humidity in the hottest month

Fig. 9 shows representative stratification phenomena of temperature and relative humidity of tomb air at 60 s, 360 s (0.1 h) and 1080 s (0.3 h) after sealing in the hottest month in two typical sections (X = 0.75 m and Y = 2 m). Similar to the closure of the

Table 6
Atmospheric components inside the M1 tomb chamber before excavation [53].

	O_2 /%	CO /nmol·mol^{-1}	CO_2 /μmol·mol^{-1}	CH_4 /nmol·mol^{-1}
Measured value	19.3 ± 0.1	458.3 ± 26.5	432.7 ± 2.7	1880.0 ± 25.2
Average background value	20.9	134.6	0.4	1814.4

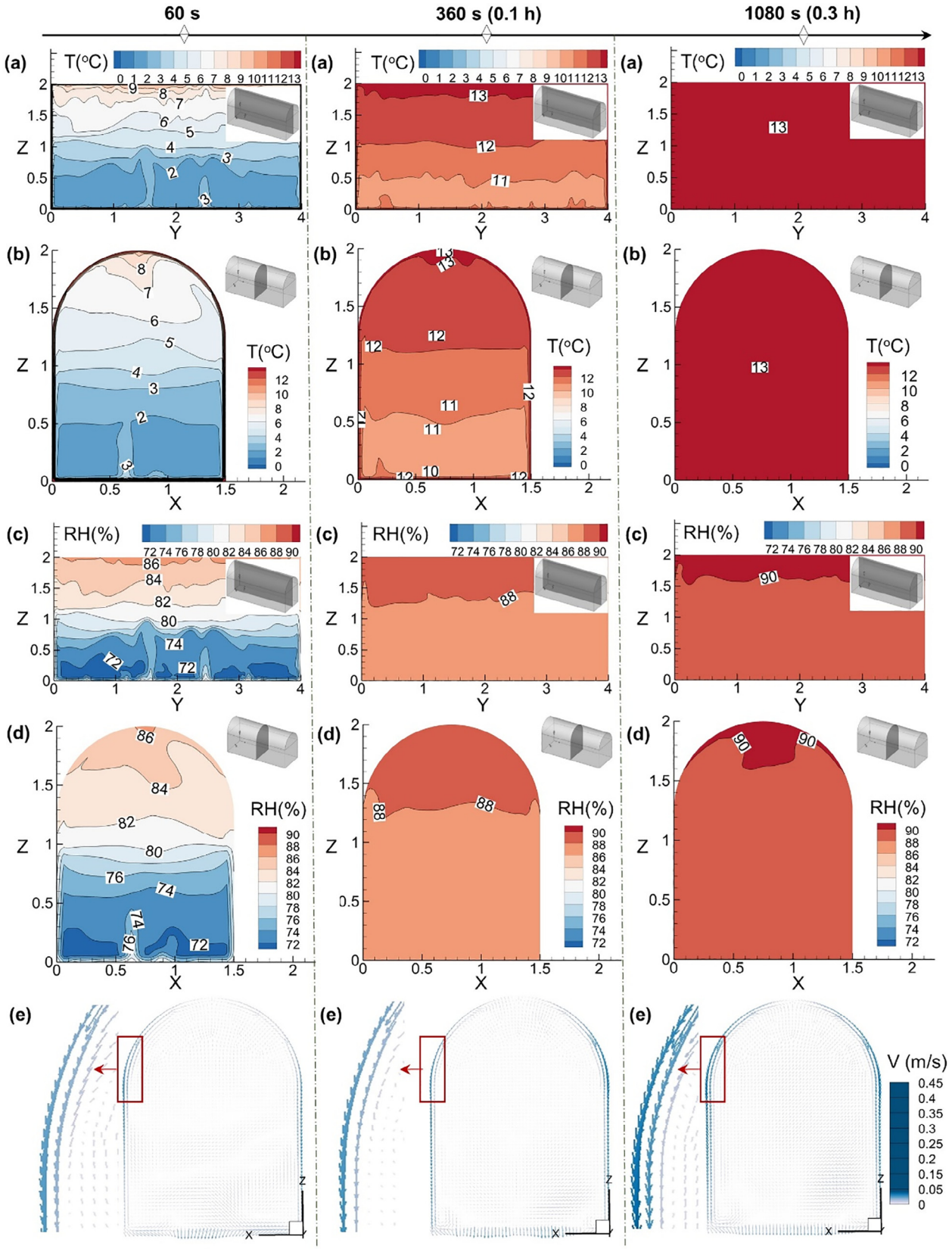

Fig. 7. Representative stratification phenomena after sealing during the coldest month. (a) T (X = 0.75 m), (b) T (Y = 2 m), (c) RH (X = 0.75 m), (d) RH (Y = 2 m), and (e) the vector of plane Y = 2 m.

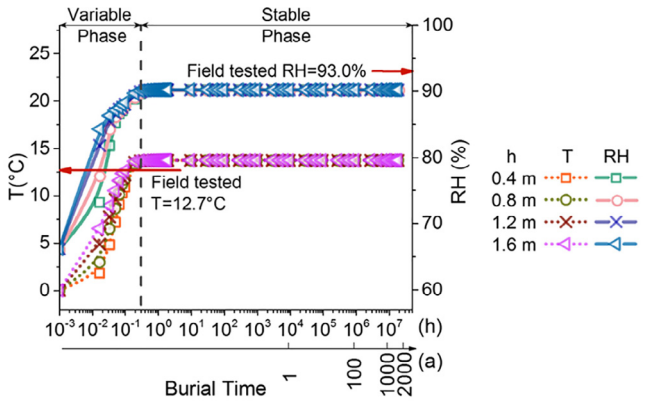

Fig. 8. Variations in average temperature and relative humidity of tomb air at four different heights in the tomb chamber after sealing during the coldest month.

tomb in the coldest month, temperature and relative humidity varied rapidly immediately after the tomb was sealed. Additionally, the velocity was very small, and the direction of the vector was upward. The stratification phenomena disappear rapidly. Variations in the average temperature and relative humidity of the tomb air at four different heights (0.4 m, 0.8 m, 1.2 m, and 1.6 m) in the tomb chamber are shown in Fig. 10. The burial time consists of a variable phase and a stable phase. The variable phase was also as short as 0.3 h. After burial, the relatively hot air still floated in the upper tomb. The temperature of the lower air gradually decreased, and the relative humidity increased under the influence of the colder wall temperature and higher soil moisture. Consequently, the temperature of the upper air gradually decreased slowly, while the temperature of the lower air decreased quickly. The relative humidity of the upper air slowly increased, while the relative humidity of the lower air quickly increased. Similarly, the temperature and relative humidity exhibited stratification in the vertical direction. The higher the height was, the higher the air temperature was. In contrast, the relative humidity was lower when the height was higher. The variable phase was from 0 h to 0.3 h, which was the same as during the coldest month. The closer to 0.3 h the phase was, the weaker the stratification phenomenon was. Finally, the air temperature of the chamber reached the same temperature as the wall, which was 13.7 °C. The variation range was 12.9 °C. The final relative humidity was 90.2%, and the variation range was 19.2%. In the last burial time, temperature and relative humidity would remain at a steady state if there was no other disturbance, such as plunder.

4. Discussion

In this paper, simulation takes the temperature and RH in the hottest and coldest months as the initial conditions. The indoor temperature and RH became stable within 0.3 h. Thus, air temperature and RH in the tomb will be stable within 0.3 h regardless of when the tomb is closed. Rapid variations in temperature and RH for the tomb air in the initial variable phase have great impacts on the integrity of historical artifacts during the burial time [47,67]. The preservation state of the lacquered wood box excavated from the M1 tomb chamber of Zhang An-shi confirmed the above expression. When the M1 tomb chamber was excavated, all that remained of the lacquered wood box was the well-preserved lacquered coating. The wood substrate underwent serious decay and was in the form of powder. One of the reasons for this decay is the fact that the two different materials (lacquer and wood) deform differently during the rapid variation period due to different coefficients of expansion as they adapt to the new microclimate conditions. Hence, the lacquer layer peeled from the wood substrate. The rapid increase in relative humidity created conditions for the rapid reproduction of microorganisms. The structure of the wood box was gradually destroyed when wood-rotting fungi decomposed cellulose and hemicellulose of the wood substrate. Shape changes of artifacts always lag behind the variations in temperature and relative humidity [11,68]. Microbial deterioration will not stop until the microclimate is unfavorable for microbial growth. Therefore, physical and microbial deterioration takes longer than changes in thermal and humid conditions.

Fortunately, in the variation phase, the overall changes in temperature and relative humidity are one-way except for little fluctuation. So, the deterioration of historical artifacts will stop finally after the closure of the tomb. If the deterioration process is very short, historical artifacts can remain in good condition until they are excavated. When historical artifacts are suddenly excavated, they must adapt to new microclimatic conditions. Deteriorations will restart, particularly when the outside environment parameters fluctuate frequently. Historical artifacts will also suffer irreversible damage.

Therefore, it is meaningful to probe the microclimate parameters before excavation. The fluctuation range of temperature and relative humidity can preliminarily predict the damage status of the objects in the tomb. The estimation of temperature and relative humidity in the tomb can provide a reference for preventive protection. An environmental chamber or inflatable "air dome" can be used to create the same temperature and RH during the excavation period. This approach is an effective method to guarantee cultural relics conserved in the same environment as the original situation [69,70]. If cultural relics are to be preserved in museums, it is advisable for a museum to build the same environment. Although many studies have determined suitable conservation parameters for various materials of cultural relics [71,72], our results deduce that the annual local average temperature is optimal for the conservation of underground artifacts excavated from the soil thermostatic layer. As a result, the conservation environment for museum collections may be different depending on the local climate. Taking Xi'an as an example, the optimal temperature for conservation may be 13 °C ± 1 °C rather than 19 °C ± 1 °C in winter or 24 °C ± 1 °C in summer, which is used in many museums [72].

However, maintaining the temperature in the museum at the annual average temperature with low energy consumption is a great challenge. High energy consumption in museums is a widespread problem. The cooling and heating consumption of the first hall of Emperor Qinshihuang's Mausoleum Site Museum is approximately 2860.66 kW and 8559.00 kW, respectively [73]. The annual cooling and heating energy consumption in a cultural property in Seoul is 29741 kW and 2648 kW [74]. Heating consumption is significantly higher than cooling consumption. Heating accounts for 70% of the energy savings of the Audain Art Museum [75].

Given the urgency of energy savings in HVAC systems in museums, much research has been conducted. Cho et al. [74] analyzed the effect of energy efficiency measure (EEM) packages, which improve the hygrothermal and energy performances using infrared thermography images and building simulations. Chang et al. [76] and Luo et al. [7] proposed an evaporative cooling system to control the local environment of the historical site. This system can create the high humidity required by the preservation of unearthed cultural relics with low energy consumption. Ramos et al. [77] designed a cost-optimal methodology for the refurbishment of historic buildings. This methodology could reduce cooling demands by more than 43% with little additional costs. Most energy consumption is used for the nonhistorical site area, as an exhibition hall only occupies a small space relative to the large space of the museum. Lucchi [78] proposed a simplified assessment method

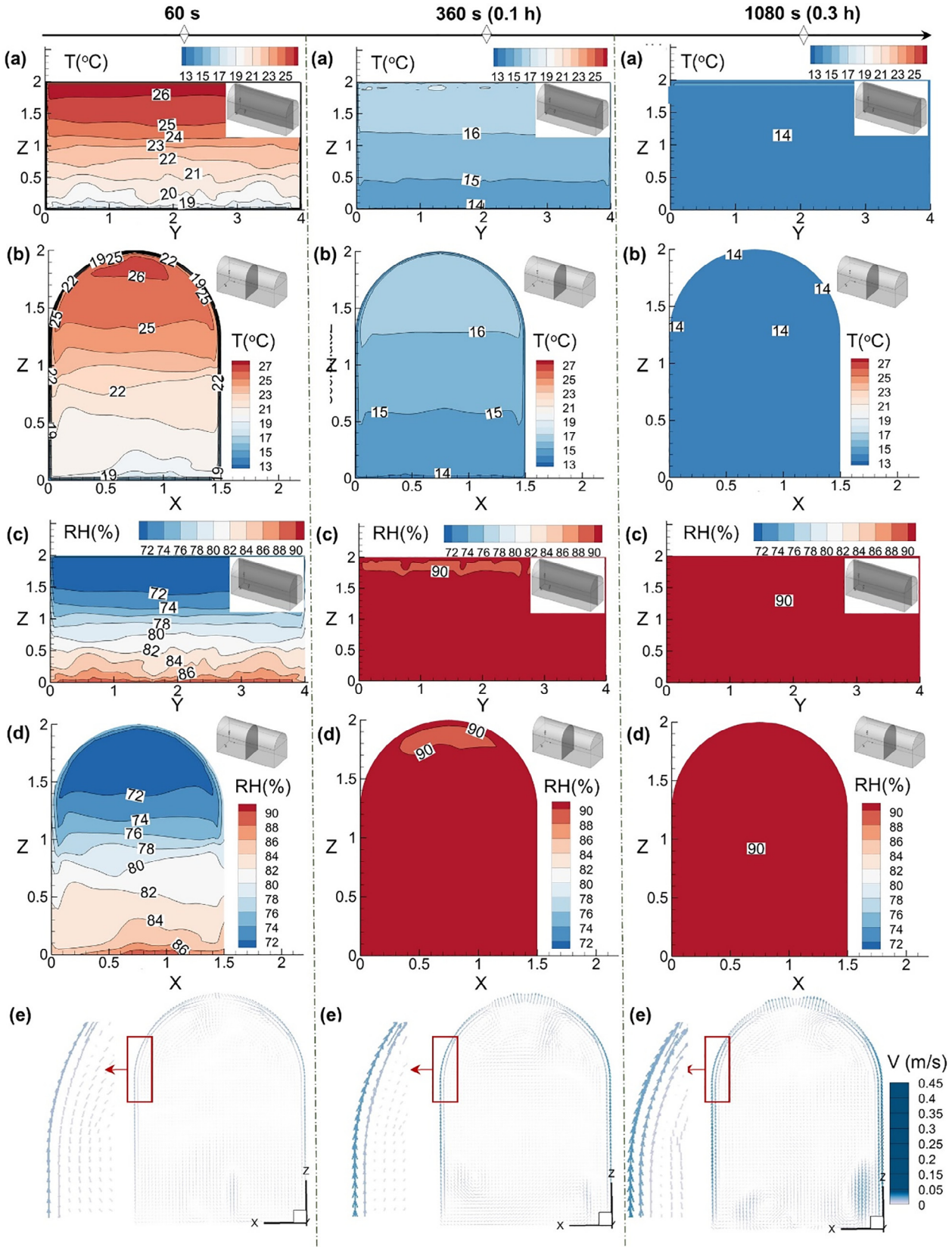

Fig. 9. Representative stratification phenomena after sealing during the hottest month. (a) T (X = 0.75 m), (b) T (Y = 2 m), (c) RH (X = 0.75 m), (d) RH (Y = 2 m), and (e) the vector of plane Y = 2 m.

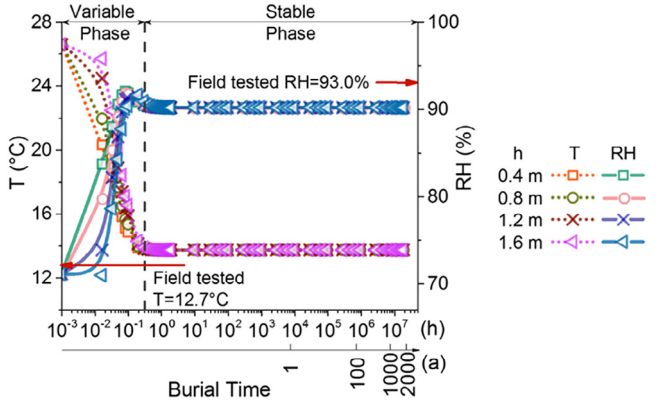

Fig. 10. Variations in average temperature and RH of tomb air at four different heights in the tomb chamber after sealing during the hottest month.

to assess the environmental and energy quality of museum buildings. It has been applied in some European museums and successfully identifies weaknesses. Sciurpi et al. [79] created a 3D energy model of the La Specola museum to evaluate retrofitting strategies. Museums are not only preservation places of cultural relics but also windows for the public to learn history [80]. The thermal comfort requirement of people is different from that of cultural relics. Schito et al. [81] applied a methodology to choose the optimal HVAC control to satisfy multiple requirements of artwork preservation, visitors' thermal comfort and energy efficiency. The high energy consumption of the HVAC system makes it unfeasible for some museums [27]. Even if there is an HVAC system in a museum, it is difficult to use for continuous operation. Therefore, the passive method is also important to maintain an appropriate temperature and RH. A novel passive method combined phase change material and silica gel to regulate air temperature and RH in museum display cases [82]. A lumped parameter model could reasonably predict the performance of a passive-type showcase environment [70]. Hygro-adsorbing plaster was adopted as an envelope material to enhance the microclimate in historic buildings. The acceptable RH range was improved from 16.1% to 33.3% [83].

For unearthed cultural relics, it suggested that newly excavated cultural relics are better preserved in the archaeological museum, which was constructed in the underground space where the relics were found. The slight temperature difference is good for not only cultural relics' preservation but also energy savings.

The 2000-year-old ancient underground tomb in this study is located in the soil thermostatic layer and was undamaged before excavation. It is still maintained in the original state of preservation. However, most tombs were likely located above the thermostatic layer. They were affected by the external environment even though they were not destroyed. Notably, for tomb chambers destroyed during the long period of burial, the artifacts are deeply influenced by the external environment. Nevertheless, characterizing the environment of the ancient tomb chamber is essential for museum environment design and cultural heritage protection or preventive conservation.

5. Conclusions

Protection of underground cultural relics is an important issue that cannot be ignored in the development of urban underground space. In this paper, the variation in the microenvironment during burial time in an ancient underground tomb was investigated by field testing and CFD modeling. The current research provided an important scientific basis for the preventive protection of cultural relics. The main conclusions of this study are as follows:

(1) The aerobic decomposition process occurred mainly in the underground tomb chamber. The main gas product is CO_2.
(2) The burial time of an ancient tomb generally consists of a short variable phase and a long stable phase. The very beginning variable phase of air temperature and relative humidity is as short as 0.3 h. The rapid variations and large differences in temperature and relative humidity at the initial burial time could determine the integrity of artifacts in long-term burial.
(3) The optimal preservation temperature for historical artifacts excavated from the soil thermostatic layer should maintain the local average annual temperature. Taking Xi'an as an example, the optimal temperature for conservation may be 13 °C ± 1 °C. The local annual temperature in the burial environment should be given more attention to ensure the sustainability of historical artifacts and the conservation environment.

CRediT authorship contribution statement

Jing Xiong: Writing – original draft, Methodology, Investigation. **Angui Li:** Conceptualization, Supervision, Funding acquisition. **Changping Liu:** Software. **Jungang Dong:** Investigation. **Bin Yang:** Writing - review & editing. **Junji Cao:** Resources. **Tong Ren:** Software, Validation.

Declaration of Competing Interest

The authors declare that they have no known competing financial interests or personal relationships that could have appeared to influence the work reported in this paper.

References

[1] J. Yu, Y. Kang, Z. Zhai, Advances in research for underground buildings: energy, thermal comfort and indoor air quality, Energy Build. 215 (2020) 109916, https://doi.org/10.1016/j.enbuild.2020.109916.
[2] E. Nezhnikova, The use of underground city space for the construction of civil residential buildings, Procedia Eng. 165 (2016) 1300–1304.
[3] Ministry of Culture and Tourism of the People's Republic of China, Statistical Yearbook of Chinese Culture and Tourism, National Library of China Publishing House, 2019.
[4] M. Botticelli, S. Mignardi, C. De Vito, Y. Liao, D. Montanari, M. Shakarna, L. Nigro, L. Medeghini, Variability in pottery production at Khalet al-Jam'a necropolis, Bethlehem (West Bank): from the Early-Middle Bronze to the Iron Age, Ceram. Int. 46 (10) (2020) 16405–16415.
[5] X. Luo, Y. Dang, C.W. Yu, Z. Gu, The practice of local environment control for the funerary pits of Emperor Qin's Mausoleum Site Museum, Indoor Built Environ. 30 (3) (2021) 293–297.
[6] A. Koh, K. Birney, Ancient organic residues as cultural and environmental proxies: the value of legacy objects, Sustainability 11 (3) (2019) 656, https://doi.org/10.3390/su11030656.
[7] X. Luo, B. Chang, W. Tian, J. Li, Z. Gu, Experimental study on local environmental control for historical site in archaeological museum by evaporative cooling system, Renewable Energy 143 (2019) 798–809.
[8] X. Luo, X. Huang, Z. Feng, J. Li, Z. Gu, Influence of air inlet/outlet arrangement of displacement ventilation on local environment control for unearthed relics within site museum, Energy Build. 246 (2021) 111116, https://doi.org/10.1016/j.enbuild.2021.111116.
[9] X. Luo, X. Zhu, W. Tian, Z. Gu, The negative impact of skylights on light-irresponsive historical sites within archaeological museums: a case study, Sol. Energy 202 (2020) 104–114.
[10] S.H. Smedemark, M. Ryhl-Svendsen, J. Toftum, Distribution of temperature, moisture and organic acids in storage facilities with heritage collections, Build. Environ. 175 (2020) 106782, https://doi.org/10.1016/j.buildenv.2020.106782.
[11] P. Brimblecombe, Temporal humidity variations in the heritage climate of South East England, Heritage Sci. 1 (1) (2013) 3, https://doi.org/10.1186/2050-7445-1-3.
[12] A. Sadlowska-Salega, J. Radon, Feasibility and limitation of calculative determination of hygrothermal conditions in historical buildings: Case study of st. Martin church in Wisniowa, Build. Environ. 186 (2020).
[13] F. Pinzari, L. Cornish, A.D. Jungblut, Skeleton bones in museum indoor environments offer niches for fungi and are affected by weathering and deposition of secondary minerals, Environ. Microbiol. 22 (1) (2020) 59–75.
[14] G. Thomson, The museum environment, Elsevier, 2013.

[15] R. Hendrickx, G. Desmarais, M. Weder, E.S.B. Ferreira, D. Derome, Moisture uptake and permeability of canvas paintings and their components, J. Cult. Heritage 19 (2016) 445–453.
[16] F. Becherini, A. Bernardi, E. Frassoldati, Microclimate inside a semi-confined environment: valuation of suitability for the conservation of heritage materials, J. Cult. Heritage 11 (4) (2010) 471–476.
[17] S. Svensson, T. Toratti, Mechanical response of wood perpendicular to grain when subjected to changes of humidity, Wood Sci. Technol. 36 (2) (2002) 145–156.
[18] J. Trovão, F. Gil, L. Catarino, F. Soares, I. Tiago, A. Portugal, Analysis of fungal deterioration phenomena in the first Portuguese King tomb using a multi-analytical approach, Int. Biodeterior. Biodegrad. 149 (2020) 104933, https://doi.org/10.1016/j.ibiod.2020.104933.
[19] Y. Li, Z. Huang, E. Petropoulos, Y. Ma, Y. Shen, Humidity governs the wall-inhabiting fungal community composition in a 1600-year tomb of Emperor Yang, Sci. Rep. 10 (1) (2020), https://doi.org/10.1038/s41598-020-65478-z.
[20] W. Ma, F. Wu, T. Tian, D. He, Q.i. Zhang, J Gu, Y. Duan, D. Ma, W. Wang, H. Feng, Fungal diversity and its contribution to the biodeterioration of mural paintings in two 1700-year-old tombs of China, Int. Biodeterior. Biodegrad. 152 (2020) 104972, https://doi.org/10.1016/j.ibiod.2020.104972.
[21] M.C. Tomassetti, A. Cirigliano, C. Arrighi, R. Negri, F. Mura, M.L. Maneschi, M.D. Gentili, M. Stirpe, C. Mazzoni, T. Rinaldi, A role for microbial selection in frescoes' deterioration in Tomba degli Scudi in Tarquinia, Italy, Sci. Rep. 7 (2017) 6027.
[22] I. Dominguez-Moñino, M. Diaz-Herraiz, V. Jurado, L. Laiz, A.Z. Miller, J.L. Santos, E. Alonso, C. Saiz-Jimenez, Nature and origin of the violet stains on the walls of a Roman tomb, Sci. Total Environ. 598 (2017) 889–899.
[23] R. Cataldo, A. De Donno, G. De Nunzio, G. Leucci, L. Nuzzo, S. Siviero, Integrated methods for analysis of deterioration of cultural heritage: the Crypt of "Cattedrale di Otranto", J. Cult. Heritage 6 (1) (2005) 29–38.
[24] D.C. Ilieș, F. Marcu, T. Caciora, L. Indrie, A. Ilieș, A. Albu, M. Costea, L. Burtă, Ș. Baias, M. Ilieș, M. Sandor, G.V. Herman, N. Hodor, G. Ilieș, Z. Berdenov, A. Huniadi, J.A. Wendt, et al., Investigations of museum indoor microclimate and air quality. Case Study from Romania, Atmosphere 12 (2) (2021) 286, https://doi.org/10.3390/atmos12020286.
[25] H. Sharif-Askari, B. Abu-Hijleh, Review of museums' indoor environment conditions studies and guidelines and their impact on the museums' artifacts and energy consumption, Build. Environ. 143 (2018) 186–195.
[26] N. Feng, Overview of preventive conservation and the museum environment in China, Stud. Conserv. 61 (sup1) (2016) 18–22.
[27] E. Schito, P. Conti, L. Urbanucci, D. Testi, Multi-objective optimization of HVAC control in museum environment for artwork preservation, visitors' thermal comfort and energy efficiency, Build. Environ. 180 (2020) 107018, https://doi.org/10.1016/j.buildenv.2020.107018.
[28] J. Ferdyn-Grygierek, K. Grygierek, Proposed strategies for improving poor hygrothermal conditions in museum exhibition rooms and their impact on energy demand, Energies 12 (4) (2019) 620, https://doi.org/10.3390/en12040620.
[29] S. Bichlmair, S. Raffler, R. Kilian, The Temperierung heating systems as a retrofitting tool for the preventive conservation of historic museums buildings and exhibits, Energy Build. 95 (2015) 80–85.
[30] X. Luo, Z. Gu, W. Tian, Y. Xia, T. Ma, Experimental study of a local ventilation strategy to protect semi-exposed relics in a site museum, Energy Build. 159 (2018) 558–571.
[31] X. Luo, Z. Gu, C. Yu, T. Ma, K. Kase, Efficacy of an air curtain system for local pit environmental control for relic preservation in archaeology museums, Indoor Built Environ. 25 (1) (2015) 29–40.
[32] X. Luo, S. Lei, W. Tian, Z. Gu, Evaluation of air curtain system orientated to local environmental control of archaeological museum: A case study for the stone armor pit of Emperor Qin's Mausoleum Museum, Sustainable Cities Soc. 57 (2020) 102121, https://doi.org/10.1016/j.scs.2020.102121.
[33] J. Ferdyn-Grygierek, K. Grygierek, HVAC control methods for drastically improved hygrothermal museum microclimates in warm season, Build. Environ. 149 (2019) 90–99.
[34] C. Saiz-Jimenez, S. Cuezva, V. Jurado, A. Fernandez-Cortes, E. Porca, D. Benavente, J.C. Canaveras, S. Sanchez-Moral, Paleolithic art in peril: policy and science collide at Altamira Cave, Science 334 (6052) (2011) 42–43.
[35] C. Cacace, G. Caneva, F. Gallo, T. Georgiadis, O. Maggi, P. Valenti, in: Cultural heritage and aerobiology, Springer Netherlands, Dordrecht, 2003, pp. 47–79.
[36] J. Elez, S. Cuezva, A. Fernandez-Cortes, E. Garcia-Anton, D. Benavente, J.C. Cañaveras, S. Sanchez-Moral, A GIS-based methodology to quantitatively define an Adjacent Protected Area in a shallow karst cavity: The case of Altamira cave, J. Environ. Manage. 118 (2013) 122–134.
[37] F. Bourges, P. Genthon, D. Genty, M. Lorblanchet, E. Mauduit, D. D'Hulst, Conservation of prehistoric caves and stability of their inner climate: lessons from Chauvet and other French caves, Sci. Total Environ. 493 (2014) 79–91.
[38] J. Zhang, L. Cai, X. Gao, M. Liu, Thought and suggestion on protection techniques of paint layers of Qin Terracotta Army, Sci. Conserv. Archaeol. 01 (2007) 51–56 (in Chinese).
[39] E. Lucchi, Review of preventive conservation in museum buildings, J. Cult. Heritage 29 (2018) 180–193.
[40] J. Xu, Y. Wei, H. Jia, L. Xiao, D. Gong, A new perspective on studying burial environment before archaeological excavation: analyzing bacterial community distribution by high-throughput sequencing, Sci. Rep. 7 (2017) 41691.
[41] D. Lacanette, D. Large, C. Ferrier, N. Aujoulat, F. Bastian, A. Denis, V. Jurado, B. Kervazo, S. Konik, R. Lastennet, et al., A laboratory cave for the study of wall degradation in rock art caves: an implementation in the Vézère area, J. Archaeol. Sci. 40 (2) (2013) 894–903.
[42] P. Fu, G. Teri, J. Li, Y. Huo, H. Yang, Y. Li, Analysis of an ancient architectural painting from the Jiangxue Palace in the Imperial Museum, Beijing, China, Anal. Lett. 54 (4) (2021) 684–697.
[43] D.J. Huisman, M.R. Manders, E.I. Kretschmar, R.K.W.M. Klaassen, N. Lamersdorf, Burial conditions and wood degradation at archaeological sites in the Netherlands, Int. Biodeterior. Biodegrad. 61 (1) (2008) 33–44.
[44] H. Xie, D. Ogura, H. Yasui, N. Takatori, S. Hokoi, S. Wakiya, A. Yanagida, Y. Kohdzuma, Environment in stone chamber of an unexcavated tumulus and preservation of buried relics: Part 1. Environmental monitoring for simulated tumulus, J. Build. Phys. 44 (4) (2021) 287–308.
[45] Z. Tong, Y. Chen, A. Malkawi, G. Adamkiewicz, J.D. Spengler, Quantifying the impact of traffic-related air pollution on the indoor air quality of a naturally ventilated building, Environ. Int. 89-90 (2016) 138–146.
[46] S.P. Corgnati, M. Perino, CFD application to optimise the ventilation strategy of Senate Room at Palazzo Madama in Turin (Italy), J. Cult. Heritage 14 (1) (2013) 62–69.
[47] D. D'Agostino, P.M. Congedo, CFD modeling and moisture dynamics implications of ventilation scenarios in historical buildings, Build. Environ. 79 (2014) 181–193.
[48] R. Zhang, Y. Zhang, K.P. Lam, D.H. Archer, A prototype mesh generation tool for CFD simulations in architecture domain, Build. Environ. 45 (10) (2010) 2253–2262.
[49] E.E. Khalil, Ventilation of the pheronic tombs of the valley of Kings, Luxor, Egyt, Int. J. Air-Condition. Refrig. 20 (1) (2012) 1150002.1–1150002.7.
[50] C. Balocco, G. Petrone, O. Maggi, G. Pasquariello, R. Albertini, C. Pasquarella, Indoor microclimatic study for Cultural Heritage protection and preventive conservation in the Palatina Library, J. Cult. Heritage 22 (2016) 956–967.
[51] D. Lacanette, S. Vincent, A. Sarthou, P. Malaurent, J.-P. Caltagirone, An Eulerian/Lagrangian method for the numerical simulation of incompressible convection flows interacting with complex obstacles: Application to the natural convection in the Lascaux cave, Int. J. Heat Mass Transf. 52 (11-12) (2009) 2528–2542.
[52] Y. Ding, Z. Zhang, Y. Zhu, Archeology of the family tomb of Zhang An-Shi, the important minister in the western Han Dynasty, Popular Archaeol. 12 (2014) 34–43 (In Chinese).
[53] J. Cao, J. Yang, T. Hu, S. Lee, X. Wang, H. Kinfai, J. Dong, Y. Ding, Investigation on atmospheric environment in M1 tomb chamber of mausoleum Zhang An-Shi, Han Dynasty, Sci. Conserv. Archaeol. 25 (02) (2013) 69–76 (In Chinese).
[54] Operation manual of landfill gas analyser LFG 20, ADC Gas Analysis Ltd. 2002.
[55] Operation and service manual of Q-Trak Indoor Air Quality Meter (Model 7565), TSI Inc. 2007.
[56] X. Zhang, Heat transfer, China Architecture & Building Press (2014).
[57] M.P. Casaletto, G.M. Ingo, M. Albini, A. Lapenna, I. Pierigè, C. Riccucci, F. Faraldi, An integrated analytical characterization of corrosion products on ornamental objects from the necropolis of Colle Badetta-Tortoreto (Teramo, Italy), Appl. Phys. A 100 (3) (2010) 801–808.
[58] Y. Zhao, R. Li, C. Ji, C. Huan, B. Zhang, L. Liu, Parametric study and design of an earth-air heat exchanger using model experiment for memorial heating and cooling, Appl. Therm. Eng. 148 (2019) 838–845.
[59] X. Liu, J. Zhao, C. Shi, B. Zhao, Study on soil thermostatic layer, Acta Energiae Solaris Sinica 28 (2007) 494–498 (In Chinese).
[60] Z. Zhang, Y. Ding, Y. Zhu, Tomb chambers of the important minister in the western Han Dynasty located in Fengqiyuan, China Cult. Heritage 6 (2011) 82–91 (In Chinese).
[61] K. Zhu, A preliminary study on climate change nearly five thousand years of China, Meteorol. Sci. Technol. S1 (1973) 15–38 (In Chinese).
[62] H. Xu, J. Guo, Analysis of temperature variation in 65 years of Xi'an, J. Shaanxi Meteorol. 1 (1998) 19–22 (In Chinese).
[63] Climatic Data Center, National Meteorological Information Center, China Meteorological Administration. http://data.cma.cn/data/detail/dataCode/A.0029.0001.html (In Chinese).
[64] D. Mathieu (Ed.), Handbook on hyperbaric medicine, Springer, 2006, 27.
[65] L. Zhou, X. Zhou, X. Zhang, Y. Wen, P. Yan, Progress in the study of background greenhouse gases at Waliguan Observatory, Acta Meteorol. Sinica 65 (2007) 458–468 (In Chinese).
[66] S. Wang, Z. Shen, L. Gu, Numerical simulation of buoyancy-driven turbulent ventilation in attic space under winter conditions, Energy Build. 47 (2012) 360–368.
[67] C.R. de Freitas, The role and importance of cave microclimate in the sustainable use and management of show caves, Acta Carsol. 39 (3) (2010).
[68] Ł. Bratasz, R. Kozłowski, D. Camuffo, E. Pagan, Impact of indoor heating on painted wood-Monitoring the altarpiece in the Church of Santa Maria Maddalena in Rocca Pietore, Italy, Stud. Conserv. 52 (3) (2007) 199–210.
[69] X. Luo, Z. Gu, T. Li, X. Meng, T. Ma, C. Yu, Environmental control strategies for the in situ preservation of unearthed relics in archaeology museums, J. Cult. Heritage 16 (6) (2015) 790–797.
[70] F. Romano, L.P.M. Colombo, M. Gaudenzi, C.M. Joppolo, L.P. Romano, Passive control of microclimate in museum display cases: A lumped parameter model and experimental tests, J. Cult. Heritage 16 (4) (2015) 413–418.
[71] Ashley-Smith J., Burmester A., Eibl M., Climate for collections-Standards and uncertainties. Postprints of the Munich Climate Conference 7 to 9 November 2012: Doerner Institut, 2013.

[72] Camuffo D., Microclimate for cultural heritage: Measurement, risk assessment, conservation, restoration, and maintenance of indoor and outdoor monuments, Elsevier, 2019.
[73] C. Cao, X. Meng, X. Liu, X. Yang, W. Hu, L. Jin, Energy analysis of relics museum buildings, Energy Procedia 75 (2015) 1809–1818.
[74] H.M. Cho, S. Yang, S. Wi, S.J. Chang, S. Kim, Hygrothermal and energy retrofit planning of masonry façade historic building used as museum and office: a cultural properties case study, Energy 201 (2020) 117607.
[75] M. On, Heating accounts for 70% of museum's energy savings, Ashrae J. 62 (7) (2020) 40–45.
[76] B. Chang, Y. Dang, X. Luo, C.W. Yu, Z. Gu, Sustainability of evaporative cooling system for environment control for preservation of unearthed historical sites within archaeological museums in China, Sustainability 12 (23) (2020).
[77] J. Sanchez Ramos, S. Alvarez Dominguez, M. Pavon Moreno, M. Guerrero Delgado, L. Romero Rodriguez, J.A. Tenorio Rios, Design of the refurbishment of historic buildings with a cost-optimal methodology: a case study, Appl. Sci.-Basel 9 (15) (2019).
[78] E. Lucchi, Simplified assessment method for environmental and energy quality in museum buildings, Energy Build. 117 (2016) 216–229.
[79] F. Sciurpi, A. Ghelli, L. Pierangioli, "La Specola" museum in Florence: Environmental monitoring and building energy simulation, Procedia Struct. Integr. 29 (2020) 16–24.
[80] D. D'Agostino, F. de' Rossi, C. Marino, F. Minichiello, F. Russo, Double plus-zero energy historic building and improvement of hygrothermal conditions for the Palaeontology Museum of Naples, J. Build. Phys. (2020).
[81] E. Schito, P. Conti, D. Testi, Multi-objective optimization of microclimate in museums for concurrent reduction of energy needs, visitors' discomfort and artwork preservation risks, Appl. Energy 224 (2018) 147–159.
[82] M. Yu, X. Zhang, Y. Zhao, X. Zhang, A novel passive method for regulating both air temperature and relative humidity of the microenvironment in museum display cases, Energies 12 (19) (2019).
[83] I. Pigliautile, V.L. Castaldo, N. Makaremi, A.L. Pisello, L.F. Cabeza, F. Cotana, On an innovative approach for microclimate enhancement and retrofit of historic buildings and artworks preservation by means of innovative thin envelope materials, J. Cult. Heritage 36 (2019) 222–231.